WELDING RESEARCH

SUPPLEMENT TO THE *WELDING JOURNAL*, OCTOBER 1991

**Sponsored by the American Welding Society and the Welding Research Council**

# A Study of Melting Efficiency in Plasma Arc and Gas Tungsten Arc Welding

*A method for selecting optimal weld schedules to minimize net heat input is derived from calorimetric measurements*

**BY P. W. FUERSCHBACH AND G. A. KNOROVSKY**

ABSTRACT. Extensive calorimetric measurements of the net heat input for the plasma arc and the gas tungsten arc welding processes in an edge weld configuration have been conducted. The experiment compared base materials with contrasting thermal diffusivities and varied the weld process control parameters, including current pulsation, in order to determine their effects on both arc and melting efficiency.

The arc efficiency for plasma arc welding was found to be lower and more variable than for gas tungsten arc welding due to the constricting torch nozzle. The melting efficiencies for the two processes were equivalent and increased with travel speed while asymptotically reaching a maximum level. At travel speeds below this level, current pulsation was found effective in increasing the melting efficiency for both processes. For many conditions, the plasma arc welding process outperformed the gas tungsten arc welding process by achieving deeper penetration for equivalent amounts of heat input.

A dimensionless parameter was determined that correlates well with the measured melting efficiencies. It was used to express all the continuous current welds with a single curve. Simple equations using this parameter and empirical data were developed, which show that the maximum melting efficiency for two-dimensional heat flow is significantly higher than for three-dimensional heat flow.

## Introduction

Reducing the heat input to the workpiece is a primary goal for weld process selection and weld schedule development in the aerospace and electronics industries where microwelding applications are widespread. In these applications, the depth of penetration is typically less than 1.0 mm and hermeticity rather than mechanical strength is the primary joining requirement. Typical microwelded components such as electromechanical relays and specialty batteries will contain glass-to-metal seals, which can readily crack from the thermal stresses induced by the welding process. In addition, the internal working parts are often very sensitive to thermal distortion and even moderate increases in temperature.

For these reasons, microwelding is often performed with the high power density welding processes such as electron beam welding (EBW) and laser beam welding (LBW) where the heat input is thought to be low and the melting efficiency[1] high. Unfortunately, the large acquisition and maintenance costs of these processes often limit their use. Consequently, gas tungsten arc welding (GTAW) is still widely used for microwelding. It is often operated in the pulsed current mode because pulsing has been shown to increase penetration and the melting efficiency of the process (Ref. 1).

Plasma arc welding (PAW) has recently been increasingly specified for microwelding. It can be a lower cost alternative to EBW and LBW when higher power density is required. The PAW process is also thought to have advantages over the GTAW process in many microwelding applications. Typical weld improvements that have been attributed to the PAW process are deeper weld penetration, faster travel speeds, and reduced thermal distortion when compared to the GTAW process (Refs. 2, 3).

Unfortunately, significant differences in the welding parameters investigated make process comparisons on the basis of net heat input difficult since neither the arc efficiency[2] nor melting efficiency of the two processes are usually known. If the dependence of these efficiencies on the PAW and GTAW process variables was better understood, then microwelding would be much more straightforward for the engineer selecting a process or developing a weld schedule. When minimizing the overall heat input to the part is a high priority, it becomes a practical matter to select those parameters which maximize melting efficiency and still produce the required weld geometry.

It was the goal of this work and an earlier study (Ref. 4) to determine the optimum GTAW and PAW process parame-

**KEY WORDS**

Plasma Arc Welding
GTAW
Melting Efficiency
Heat Input
Weld Schedule
Measurement
Arc Efficiency
Penetration
Calorimeter

*P. W. FUERSCHBACH and G. A. KNOROVSKY are with Sandia National Laboratories, Albuquerque, N. Mex.*

1. *Melting efficiency is defined here as the amount of heat necessary to just melt the fusion zone divided by the net heat input to the part.*

2. *Arc efficiency is defined here as the net heat input to the part divided by the net machine output energy. For nonarc processes such as LBW it is called the energy transfer efficiency.*

ters for both pulsed and continuous current in order to maximize melting efficiency for the edge weld geometry examined here. Edge welds were chosen since they are commonly used in microwelded components to minimize the restraint on the weld and to confine the thermal effects in a localized region. Keyhole welding with the PAW process was not possible with this geometry and therefore only partial penetration welds were made. It was felt that only after the PAW and GTAW process parameters were optimized in terms of melting efficiency for this common microwelding geometry could a direct and reasonable comparison be made between the two processes for microwelding applications. Two materials (304 SS and Ni 200) with significantly different thermal diffusivities ($\alpha$ = 0.041 and 0.220 $cm^2/s$, respectively) were examined in order to extend the applicability of the results to a broad range of materials and to see what effect the thermal properties of a material have on melting efficiency.

## Experimental

Electrode negative (straight polarity) GTA and PA welds were made on 1.3 × 25 × 127 mm (0.05 × 1.0 × 5 in.) machined test specimens of Type 304 or 304L stainless steel and Type Ni 200. Two such pieces were joined in a standing edge weld geometry (*e.g.*, Fig. 17). The 304 and 304L stainless steels contained very similar sulfur levels: 0.007 and 0.008 wt-%, respectively, and were expected to produce weld geometries having similar depth-to-width ratios.

The test specimens and edge weld mounting fixture were attached to the bottom surface of a Seebeck envelope calorimeter[3] as shown in Fig. 1. A CNC-controlled XY table translated the calorimeter and specimens under the welding torch. The calorimeter is box shaped with internal dimensions 150 × 150 × 75 mm (6 × 6 × 3 in.). The calorimeter was left open during welding and closed immediately after the weld was completed. The calorimeter walls are maintained at room temperature with a constant temperature bath. The calorimeter operates on the gradient layer principle (Ref. 5) and produces a voltage output that is proportional to the flux through the walls during the time required for the weld samples and fixture to cool to room temperature. The energy losses with this experimental technique due to radiation, convection and evaporation have been estimated to be 1% or less of the arc energy; in addition, a very linear response has been verified for different time durations and heat input levels (Ref. 6).

The welding power supply used was the same for both processes. It is a transistor-controlled constant current, 300-A machine custom built for GTAW research applications. The frequency response of this machine is such that true square waves were obtained. This enabled accurate calculations of average and RMS current to be made using the machine settings. A supplementary pilot arc supply, deionized water cooler, and mass flow orifice gas controller enabled PAW operation.

For most of the experimental conditions, the arc voltage was measured between the torch and workpiece and recorded for the entire weld duration with a digital storage oscilloscope and stored on a floppy disk. The weld current was measured with a Hall effect current transducer on the ground return cable and stored using the second channel of the oscilloscope. Arc output energy in joules was determined by multiplying the voltage and current waveforms together and integrating the resulting power waveform for the weld period using software internal to the oscilloscope.

The output voltage of the calorimeter was recorded on another digital storage oscilloscope with a long duration trace. When the mass inside the calorimeter reached the temperature of the water bath, the output voltage became zero. The output voltage vs. time trace was then integrated to determine the energy in joules absorbed by the workpiece during the weld (*i.e.*, the net heat input). The reported values of arc efficiency were calculated by dividing the net heat input in joules by the arc output energy in joules. Weld cross-sectional area was determined (using a planimeter) from the average of four transverse metallographic sections taken from each weld. These areas were multiplied by the weld length (95 mm; 3.7 in.) to determine the total fusion zone volume. Weld penetration was measured at the joint interface from the fusion zone surface to the weld root.

The enthalpy of the weld volume was determined by multiplying the fusion zone volume by the enthalpy change ($\delta h$) required to bring a unit volume of the metal from room temperature (RT), to the liquid state at the melting point (MP). It is given by the following expression and includes the heat of fusion ($\Delta h_f$), and the sensible heat:

$$\delta h = \Delta h_f + \int_{RT}^{MP} c_p\,(T)\,dT \qquad (1)$$

Since the specific heat ($c_p$), is a function of temperature, empirical, not calculated values were used. For Ni 200 $\delta h$ was 9.87 $J/mm^3$ (Ref. 7) and for 304 and 304L stainless steel $\delta h$ was 8.70 $J/mm^3$ (Ref. 8). The reported values of melting efficiency were calculated by dividing the enthalpy of the weld volume in joules by the net heat input in joules.

The GTAW experimental conditions are shown in Table 1. Preliminary welds were made to determine the highest current and fastest travel speeds possible without causing humping of the weld bead. High travel speeds have been prescribed to increase melting efficiency (Ref. 9) and humping is known to be the practical welding speed limit in GTAW welding (Ref. 10). The nominal machine output (product of arc voltage times current divided by travel speed) was measured for this high-speed condition and then kept constant for each material (as shown in Table 1) in the continuous current experiments by varing the current and

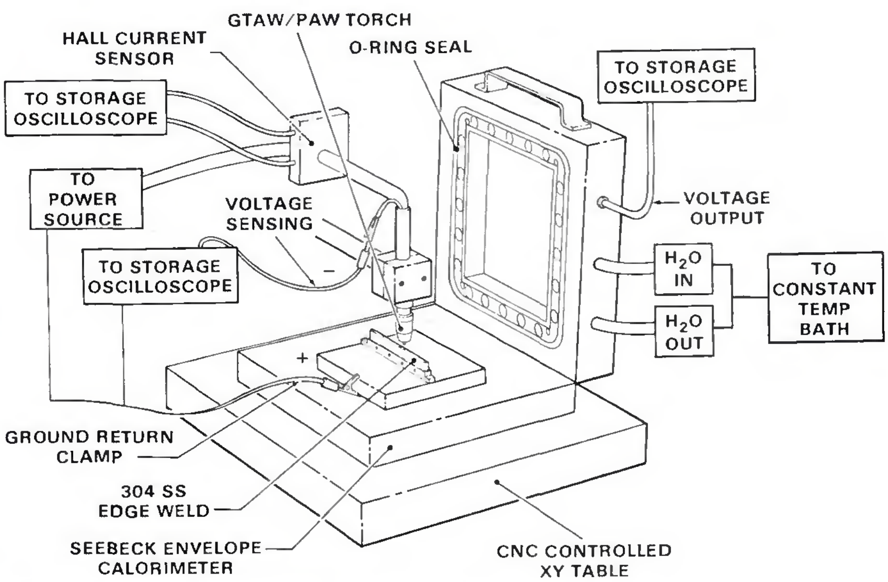


*Fig. 1 — Experimental setup for both PAW and GTAW torches.*

3. *Manufactured by Thermonetics Corp., San Diego, Calif.*

travel speed proportionally.

This nominal machine output value was also kept constant for the pulsed current welds, where two weld speeds were investigated for each material. The weld speeds were selected based on the continuous current melting efficiency results, in order to select a weld speed and melting efficiency level that could be improved by pulsing. That is, the welding speeds chosen for the pulsed current welds did not produce the maximum melting efficiency for continuous current and it was anticipated that pulsed current might have its strongest effect at these intermediate speeds. The average current levels shown in Table 1 for the pulsed welds were chosen to produce the same nominal machine output levels used for the continuous current welds. The duty cycle from Equation 2 indicates the fraction of time during a welding pulse that the current is at the peak level. A duty cycle of 1.0 is a continuous current weld made at the average current level. The average current was determined from Equation 3 and differs from the RMS current which is determined by Equation 4. The experiment was designed using only the average current values. The RMS current was calculated for some welds for comparison purposes since it reflects the maximum amplitude to a greater extent.

$$\text{Duty Cycle} = t_p/(t_p + t_b) \quad (2)$$

$$\text{Average Current} = (I_p t_p + I_b t_b)/(t_p + t_b) \quad (3)$$

$$\text{RMS Current} = [(I_p^2 t_p + I_b^2 t_b)/(t_p + t_b)]^{1/2} \quad (4)$$

where: $I_p$ = peak current; $I_b$ = background current; $t_p$ = time at peak current; and $t_b$ = time at background current.

The background current was always maintained at a low level sufficient for arc stability. The frequency of pulsing was chosen to obtain approximately a 70% spot overlap and was set proportional to travel speed as shown in Table 1. The lowest level of duty cycle used for a specific average current was limited by humping of the weld bead. All welds made in this study exhibited smooth weld bead geometries.

The PAW experimental conditions are shown in Table 2. The experimental strategy was basically the same as described above for the GTAW experiments. One difference was that the value of average current used for the pulsed current experiment was chosen to produce a lower level of nominal machine output than the continuous current experiment. This was necessary because current pulsing at higher levels resulted in melted PAW torch nozzles. The maximum allowable current that a nozzle can withstand without melting is proportional to the nozzle orifice diameter. Since the constriction of the plasma arc by the nozzle is thought to increase the power density, the smallest practical orifice diameters were always used. For the continuous current welds, this required using a different orifice diameter for each current and travel speed combination. For the pulsed current welds, the orifice diameter was kept constant for each average current in order to distinguish differences due solely to the pulsing parameters. An argon-5% hydrogen shielding gas was used exclusively for the PAW experiments because some torch manufacturers strongly recommend it in order to fully develop the constriction effect possible with their torch designs (Ref. 11).

**Table 1—GTAW Experimental Conditions**

| Alloy | 304L SS | | Nickel 200 | |
|---|---|---|---|---|
| Shielding gas | Argon | | | |
| Torch | Linde HW-9 | | Linde HW-26 | |
| Electrode diameter (mm) | 1.6 | | 2.4 | |
| Arc length (mm) | 1.0 | | | |
| **Continuous Current Experiments** | | | | |
| Machine output (J/mm) | 60 | | 80 | |
| Current range (A) | 29–132 | | 38–205 | |
| Travel speed range (mm/s) | 4.2–21.2 | | 4.2–25.4 | |
| **Pulsed Current Experiments** | | | | |
| Machine output (J/mm) | 60 | | 80 | |
| Travel Speed (mm/s) | 6.3 | 12.7 | 10.6 | 21.2 |
| Average current (A) | 42 | 81 | 83 | 167 |
| Background current (A) | 5–7 | | | |
| Duty cycle range | 0.2–1.0 | 0.4–1.0 | 0.28–1.0 | 0.67–1.0 |
| Pulse rate (Hz) | 8.3 | 16.7 | 13.9 | 27.8 |

## Results

### Arc Efficiency

For the continuous current welds, the dependence of arc efficiency on travel speed (and consequently current) for both weld processes and the two materials is shown in Fig. 2. The weld material apparently has no effect on the measured arc efficiency for either process over a wide range of arc conditions. The GTAW process exhibits a nearly constant level of arc efficiency for the experiment with the exception of the slowest travel speeds where a slight decrease is noted. Also apparent in the figure is the significantly lower level of arc efficiency found for the PAW process when compared with the GTAW process. The PAW process also differs in that it shows a trend toward higher arc efficiencies as travel speed increases and a slight decrease at the highest travel speed.

Similar levels of arc efficiency were found for the pulsed current welds where the independent variable was duty cycle instead of weld speed. As shown in Fig. 3 for pulsed GTAW, arc efficiency remains relatively constant for large changes in duty cycle, which, from Equation 3, cor-

**Table 2—PAW Experimental Conditions**

| Alloy | 304 and 304L SS[a] | | Nickel 200 |
|---|---|---|---|
| Shielding gas | Ar-5% $H_2$ | | |
| Orifice gas | Argon | | |
| Torch | Secheron (50 A) | | Thermal arc (100 A) |
| Torch standoff distance | 1.0 mm | | |
| **Continuous Current Experiments** | | | |
| Machine output (J/mm) | 60 | | 80 |
| Travel speed (mm/s) | 4.1–16.9 | | 7.6–25.4 |
| Current range (A) | 17–55 | | 30–100 |
| Orifice diameter range (mm) | 0.8–1.8 | | 0.8–2.1 |
| Orifice flow rate range (L/min) | 0.25–0.55 | | 0.25–0.80 |
| **Pulsed Current Experiments** | | | |
| Machine output (J/mm) | 45 | — | |
| Travel speed (mm/s) | 6.35 | 12.7 | |
| Average current (A) | 18 | 36 | |
| Background current (A) | 5 | 5 | |
| Duty cycle range | 0.2–1.0 | 0.44–1.0 | |
| Pulse rate (Hz) | 8.33 | 16.7 | |
| Orifice diameter (mm) | 1.5 | 1.8 | |
| Orifice flow rate (L/min) | 0.45 | 0.65 | |

*The continuous current welds were made on 304L SS and the pulsed current welds were made on 304 SS.

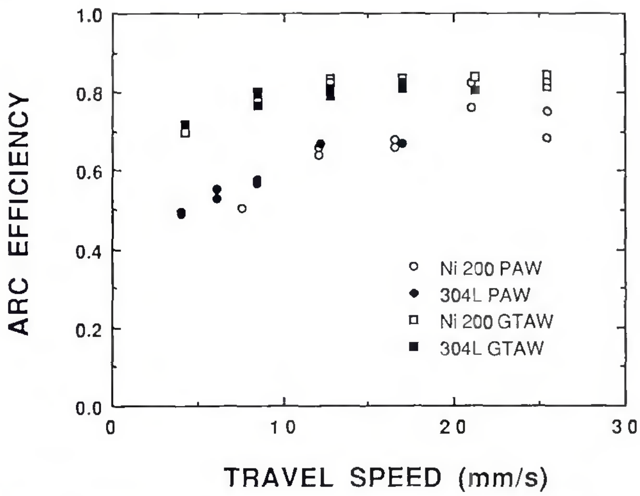


Fig. 2 — *Variation in arc efficiency due to material and weld schedule for the continuous current PAW and GTAW processes.*

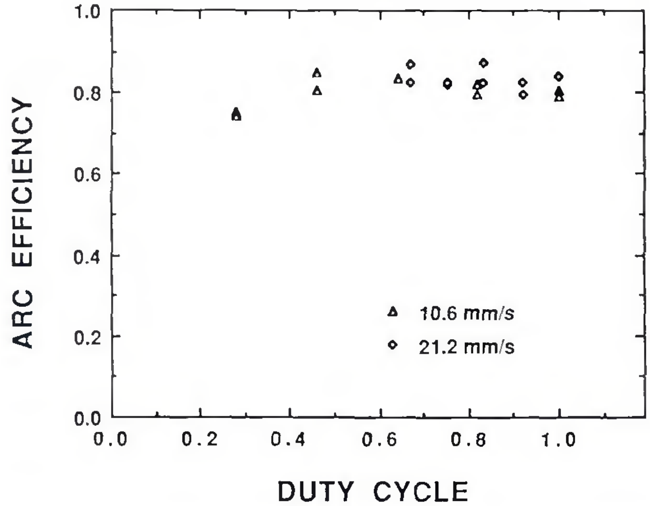


Fig. 3 — *Effect of pulsed current on arc efficiency for the GTAW process on Ni 200.*

responds to substantial changes in the peak current levels. Also note that data points corresponding to duty cycles equal to 1.0 are continuous current welds and yet are indistinguishable from the pulsed current welds in the same figure. As was seen for the continuous current PAW welds, the values of arc efficiency shown in Fig. 4 for the pulsed current PAW process are not as constant as the pulsed GTAW process and exhibit a gradual decrease in arc efficiency with decreasing duty cycle.

The two levels of weld speed shown in each figure were chosen to produce the same nominal level of machine output; consequently, because of their factor of two difference in weld speed, their average currents also differ by the same ratio. Arc efficiency for pulsed current GTAW is therefore found to be independent of average current as well as duty cycle. Comparison of Figs. 3 and 4 also reveals that the arc efficiency for the pulsed current PAW process is lower than the pulsed current GTAW process as was the case for the continuous current welds noted above.

### Heat Input

As mentioned above, it was the intention of the experimental design to make all welds of the same material at the same nominal machine output. For the continuous current welds, this resulted in net heat inputs that were relatively constant for each material. For the GTAW process, this constancy is shown in Fig. 5 where the linear heat input (calorimetrically measured heat input in joules divided by the weld length) is plotted against travel speed for both 304 stainless steel and Ni 200. Similar results were obtained for the continuous current PAW welds, signifying that nominal machine output is a strong indicator of the actual heat input to the part.

For the pulsed current welds, the average current (as calculated from Equation 3) was used to determine the nominal machine output. The resulting net heat inputs for the pulsed current GTAW welds were not as constant as the continuous current GTAW welds and were found to correlate with the RMS current instead of the average current as shown in Fig. 6 for 304 stainless steel. Also shown in this figure are the pulsed current PAW welds for 304 stainless steel, which do not demonstrate the same dependence for linear heat input on RMS current but instead are more nearly constant for a fixed average current.

### Melting Efficiency

The melting efficiencies found for the PAW and GTAW processes were quite similar. Figures 7 and 8 show that for the continuous current welds on both 304L stainless steel and Ni 200 the melting effi-

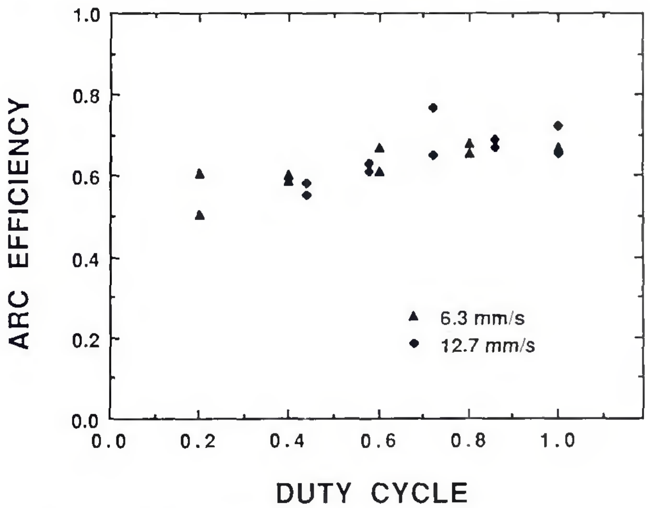


Fig. 4 — *Effect of pulsed current on arc efficiency for the PAW process on 304 stainless steel.*

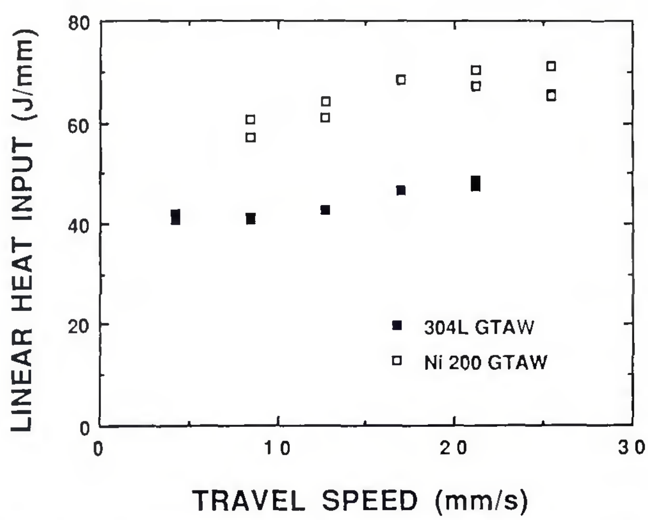


Fig. 5 — *Dependence of measured heat input on travel speed for the continuous current GTAW process.*

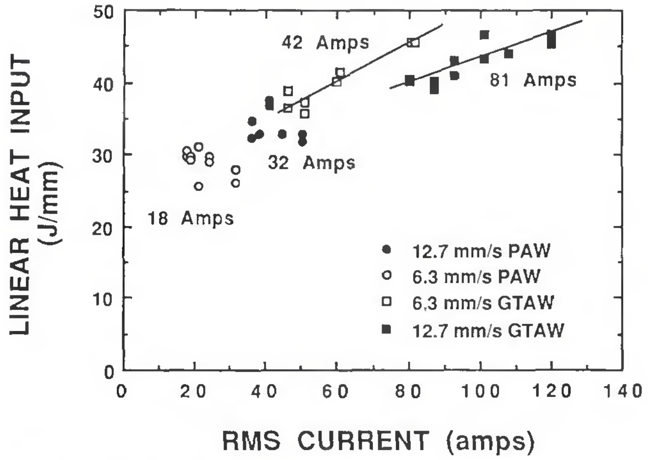


*Fig. 6 — Dependence of heat input on RMS current for pulsed current GTAW and PAW at four levels of average current on stainless steel.*

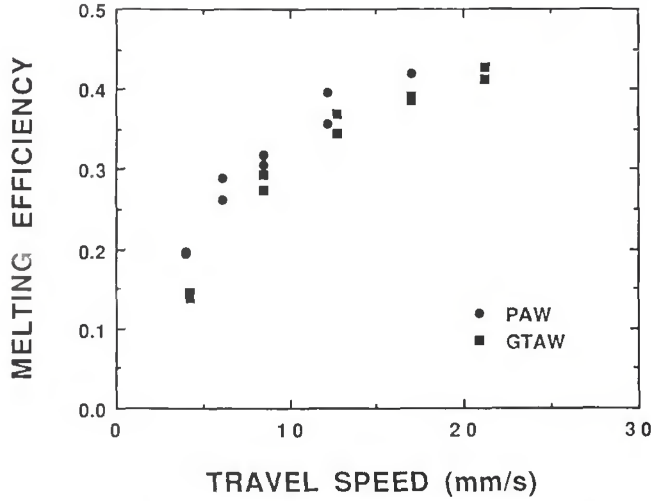


*Fig. 7 — Similar dependence of melting efficiency on travel speed for continuous current PAW and GTAW on 304L stainless steel.*

ciency for both processes increased rapidly with travel speed and tended to level off at the highest travel speeds investigated. Note the similarity in melting efficiency values for the two welding processes over a wide range of welding speeds. When all the continuous current welds (for both processes and materials) are plotted together as in Fig. 9, it becomes apparent that the measured melting efficiency for 304 stainless steel is significantly higher than that for Ni 200 at equivalent travel speeds, but both approach a common asymptotic level at high travel speeds.

For the pulsed current welds, the dependence of melting efficiency on the independent variable duty cycle was especially instructive. Figure 10 shows that for the pulsed current GTAW welds on 304 stainless steel a dichotomy exists in the relationship between melting efficiency and duty cycle for the two travel speeds tested. The melting efficiency for the slower travel speed (6.35 mm/s; 15 in./min) decreases with increasing duty cycle, whereas for the faster travel speed (12.7 mm/s; 30 in./min), the melting efficiency is relatively constant at a higher level.

The same apparent behavior was seen to a lesser extent for the pulsed current GTAW welds on Ni 200 shown in Fig. 11. A gradual decrease in melting efficiency occurred at the slower travel speed (10.6 mm/s; 25 in./min) with no consistent deviation at the higher travel speed (21.2 mm/s; 50 in./min). For the stainless steel, it is interesting to note that the peak level of melting efficiency reached at the slow travel speed is the same high level obtained for all the welds made at the faster travel speed.

In contrast to the pulsed current GTAW welds, no dichotomy exists for the pulsed current PAW welds on 304 stainless steel, since no plateau value for melting efficiency was reached at either weld speed. As shown in Fig. 12, melting efficiency varied inversely with duty cycle for both of the weld speeds investigated. It is also important to note for these pulsed current welds (Figs. 10–12), that as was found for continuous current welding, melting efficiency was usually higher at faster travel speeds.

### Penetration

Mechanical designers often specify weld strength requirements by the depth of penetration; and therefore, values of melting efficiency based on weld area may not always be a desirable means of comparison. A more practical parameter for these cases is obtained by dividing the depth of penetration by the actual measured linear heat input in order to determine how well, from a thermal efficiency perspective, penetration is achieved. Figures 13 and 14 show the dependence of this normalized penetration parameter on travel speed for continuous current welds, while Figs. 15 and 16 show its dependence on duty cycle for pulsed current welds. For many conditions, the normalized penetration was greater for the continuous

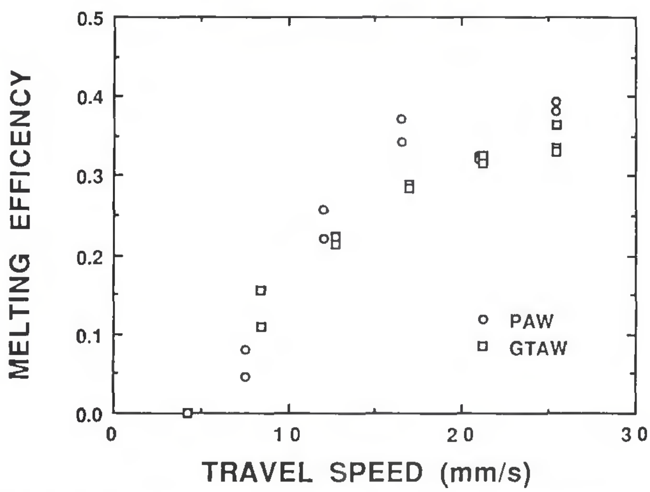


*Fig. 8 — Similar dependence of melting efficiency on travel speed for continuous current PAW and GTAW on Ni 200.*

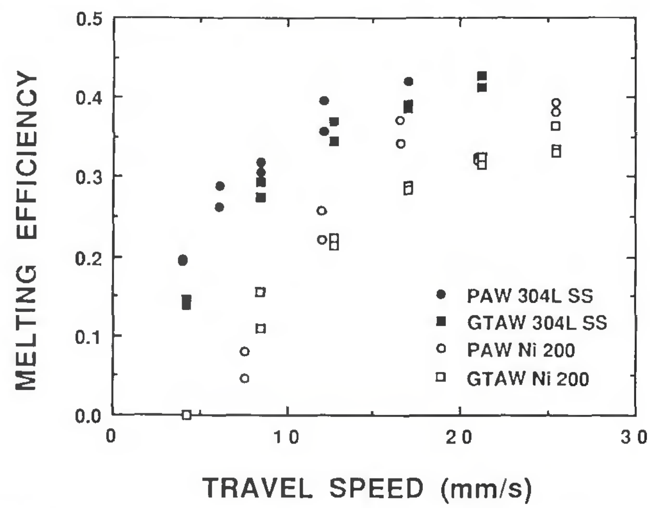


*Fig. 9 — Dependence of melting efficiency on type of base material.*

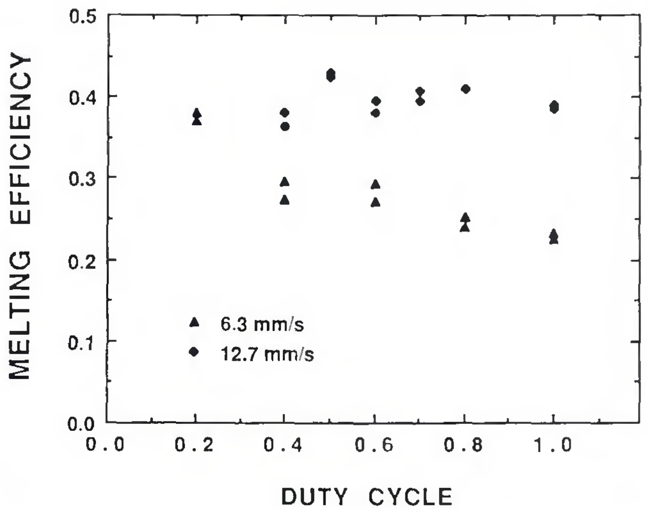


*Fig. 10 — Effect of current pulsation on GTAW melting efficiency at two welding speeds on 304L stainless steel.*

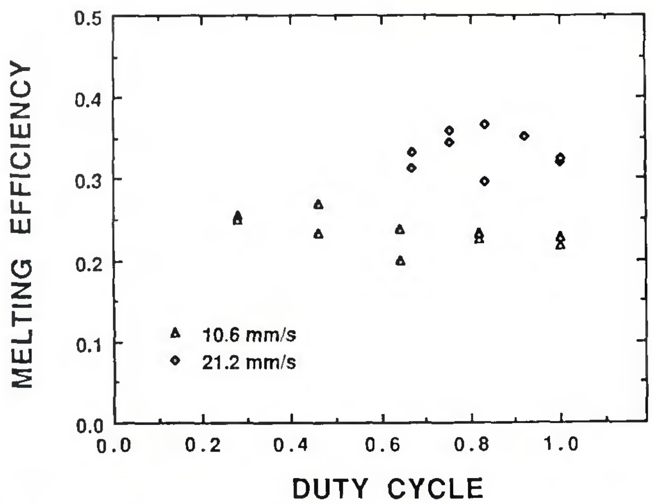


*Fig. 11 — Effect of current pulsation on GTAW melting efficiency at two welding speeds on Ni 200.*

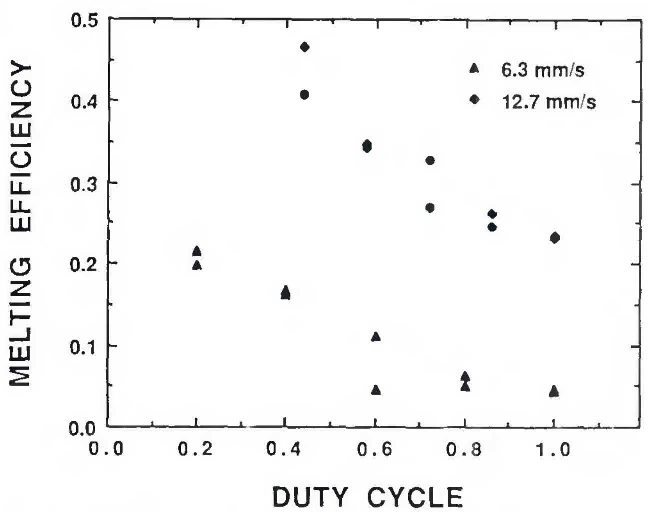


*Fig. 12 — Effect of current pulsation on PAW melting efficiency at two welding speeds on 304 stainless steel.*

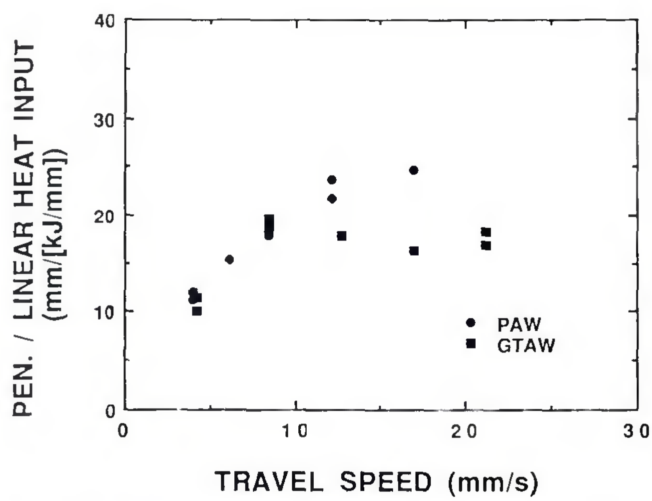


*Fig. 13 — Dependence of normalized penetration on travel speed for the continuous current GTAW and PAW processes for 304L stainless steel.*

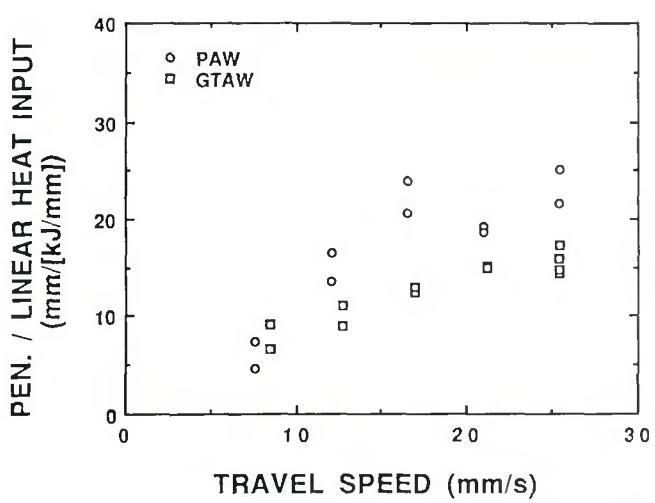


*Fig. 14 — Dependence of normalized penetration on travel speed for the continuous current GTAW and PAW processes on Ni 200.*

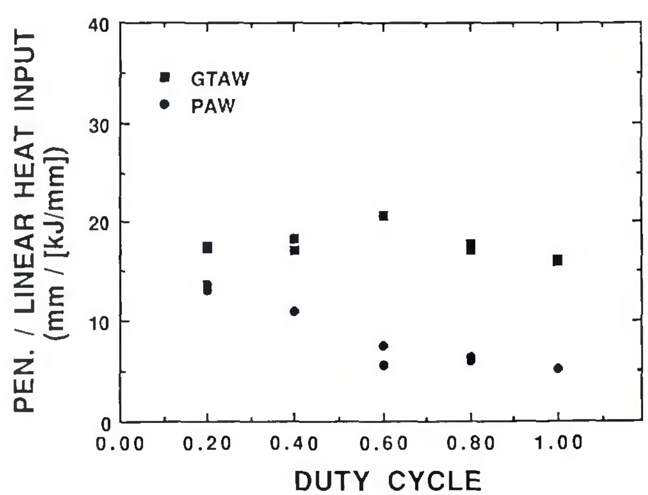


*Fig. 15 — Effect of current pulsation on normalized weld penetration in stainless steel (travel speed = 6.3 mm/s).*

current PAW process than for the continuous current GTAW process. When compared at equivalent travel speeds, the actual penetration data show that the PAW process yielded deeper penetration for equal or even lower heat inputs, which is consistent with the results shown in Figs. 13 and 14.

The increased penetration is also apparent by comparison of the metallographic cross-sections shown in Figs. 17 and 18 for continuous current welds on 304 stainless steel. The micrographs indicate that the PAW process produced deeper weld penetration at equivalent levels of travel speed and nominal heat input, where the GTAW process produced a kidney-shaped weld pool.

For the pulsed current welds shown in Figs. 15 and 16, the normalized penetration parameter for the GTAW process was relatively unaffected by duty cycle at both slow and fast travel speeds. In contrast, the PAW process showed a strong increase at the lower duty cycles indicating a beneficial effect of pulsing for these conditions.

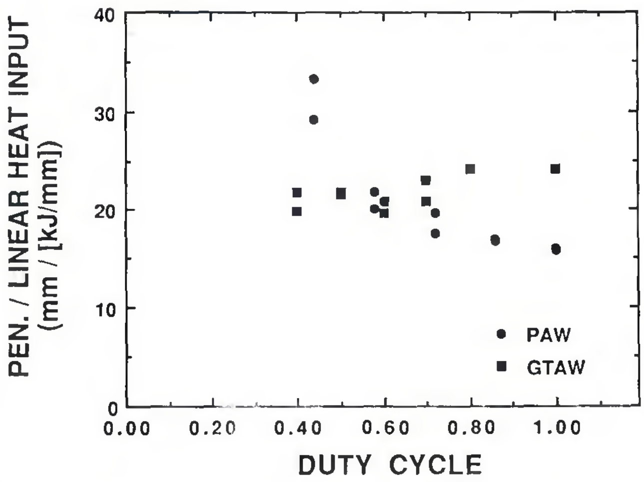


*Fig. 16 — Effect of current pulsation on normalized weld penetration in stainless steel (travel speed = 12.7 mm/s).*

## Discussion

### Arc Efficiency

The relative insensitivity of the GTAW arc efficiency to travel speed (and consequently the current amplitude) as shown in Fig. 2, has been reported earlier (Ref. 6) and can be explained by using the energy balance determined by Quigley, *et al.* (Ref. 12), for the GTAW arc, which showed that approximately 89% of the energy transfer is by the electrons. Clearly then, total current will be the dominant parameter in the arc energy balance with convective and radiative losses of secondary importance. There does appear to be a slight decrease in arc efficiency at the slowest travel speeds, which may be due to the higher arc voltages which resulted from the small weld pool size seen for these conditions. Smartt, *et al.* (Ref. 13), has shown that the GTAW arc efficiency decreases with increasing arc voltage. He also reported an arc efficiency value of about 75% for 304 stainless steels, which is in good agreement with our results where for most conditions the voltage averaged only about 8 V and the GTAW arc efficiency was about 80%.

The lack of dependence of arc efficiency on anode material appears to indicate that the work functions in a GTAW arc for the two materials are similar since the anode work function is believed to strongly affect the GTAW arc efficiency. The previously mentioned energy balance estimated that 60% of the energy transferred is due to the work function. Additionally, the similarity in arc efficiency for 304 stainless steel and Ni 200 suggests that little if any difference in arc efficiency would be expected when welding other iron- and nickel-based alloys.

Based on the above electron transfer arguments and the physical similarities between the GTAW and PAW processes, the dependence of arc efficiency on travel speed for the PAW process shown in Fig. 2 was surprising. In addition, the lower levels of arc efficiency found for the PAW process when compared to the GTAW process conflict with the theoretical results of Metcalfe and Quigley (Ref. 14) who proposed that the high gas flowrates of the PAW process would produce greater convective heat transfer at the anode and, consequently, higher arc efficiencies than the GTAW process.

We postulate that the lower arc efficiency seen for the PAW process when compared with the GTAW process is due to heat transfer at the torch nozzle which cannot occur with the GTAW process since no nozzle is present. We base this postulation on the following observations:

First, as weld speed was decreased, the current and orifice diameter were also decreased in order to optimize the arc constriction. The increased surface-to-volume ratio present for the smaller orifice diameters likely caused an increased fraction of heat transfer to the nozzle in the arc energy balance and hence, the decreased arc efficiencies seen in Fig. 2.

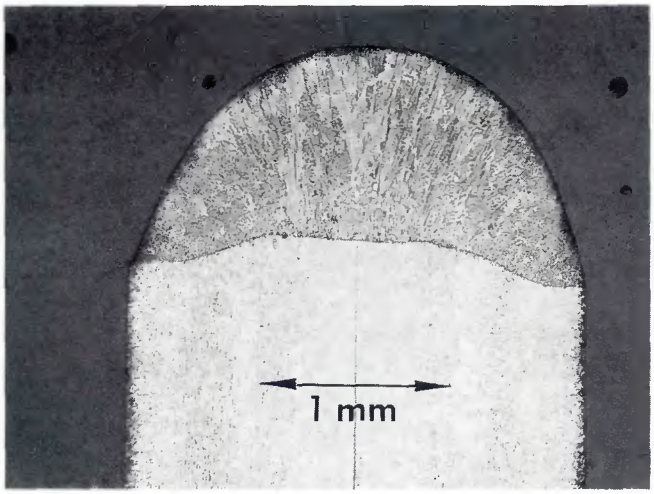


*Fig. 17 — Fusion zone cross-section in 304 SS for cont. current PAW indicating optimum penetration (machine output = 60 J/mm)*

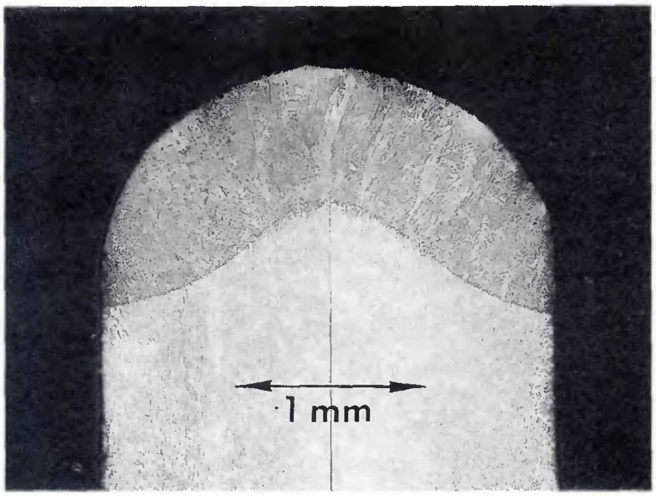


*Fig. 18 — Fusion zone cross-section in 304 SS for continuous current GTAW indicating nonoptimized melting (machine output = 60 J/mm).*

Secondly, the slight drop in arc efficiency that occurred at the highest travel speed for the continous current nickel PA welds can also be readily explained by increased nozzle heat transfer. Since a larger diameter nozzle was not available for this highest current level, the nozzle was not changed from the preceding current level. This resulted in increased current density and likely more convective cooling at the nozzle.

Thirdly, the melted water-cooled copper nozzles that occur when the current density is too high are a dramatic indication that substantial energy can be transferred away from the arc with the PAW process.

The insensitivity of arc efficiency to duty cycle for the pulsed GTAW process seen in Fig. 3 is again explained by electron transfer considerations in the same manner as for the continuous current welds discussed above. Furthermore, the levels of arc efficiency found for pulsed current are indistinguishable from those found for continuous current (duty cycle = 1.0) in Fig. 3. Because a change in duty cycle results in a change in peak current as well as a change in the fraction of time at peak current, a wide range of pulsing parameters are represented in Fig. 3. None of these parameter changes, however, significantly affected the arc efficiency of the GTAW process.

The slight increase in arc efficiency with increasing duty cycle observed for the pulsed PAW process in Fig. 4 can again be explained by the postulated convective cooling at the nozzle. Since the same nozzle diameter was used for all welds of a given weld speed, the high duty cycle welds will necessarily have lower current densities than the low duty cycle welds. The increased heat transfer that is likely to occur at the nozzle for the higher current densities will then result in reduced arc efficiency. Also note that there is little difference between the arc efficiencies for the two travel speeds in Fig. 4 despite the large change in the average current levels (Table 2). This is explained by the increased nozzle diameter at the higher travel speed which compensates for the higher current levels and likely results in similar current densities at the nozzle.

#### Heat Input

Due to the constancy of arc efficiency noted above, the measured heat inputs for the continuous current welds were also mainly constant since the machine output was not varied and the current regulation is very stable. Since no arc voltage control was used there was a slight decrease in heat input at the slower travel speeds due to the increased arc voltages noted earlier. But overall, the net heat input to the part was about the same for a wide range of currents and travel speeds (Table 2). This is an important result, because one important measure of a quality manufacturing process is the ability to adjust the process and be confident that the results are as predicted by theory. For the GTAW process, changes in net heat input can be predicted within a narrow range, despite large changes in current and travel speed, and without precise knowledge of the actual arc efficiency. In contrast, the substantial variation in energy transfer efficiency that occurs with the LBW process (Ref. 15) is a serious handicap to the welding engineer attempting to change a weld schedule since the net heat input is necessarily difficult to estimate.

For the pulsed current GTA welds as shown in Fig. 6 for 304L stainless steel, it appears that the RMS current more accurately predicts the weld heat input than does average current (which was held constant). The heat input is seen to increase with increasing RMS current, and from Equation 4, with decreasing duty cycle. Examination of voltage and current waveforms reveals that the heat input increases because the arc voltage during the peak pulse time rapidly rises in order to maintain the peak current level. This leads to an increase in machine output and consequently, the weld heat input. But as noted above and shown in Fig. 3, the arc efficiency remains constant for these pulsed GTA welds since the increased heat input is matched by a similar increase in machine output. The use of RMS current instead of average current as an indicator of actual weld heat input for pulsed current GTA welds appears to be valid since it weights the peak current amplitude to a greater degree and thereby corrects for the increased voltage that occurs.

Similar increases in voltage and machine output occurred for the pulsed current PAW welds also shown in Fig. 6. However, in this case there is no correlation of net heat input with RMS current, which is consistent with the slight decrease in arc efficiency for these welds noted earlier in Fig. 4. If the postulated increased convective cooling at the nozzle did not occur at the lower duty cycles, the heat input would probably increase as it did for the GTA welds and the RMS current would be the better indicator of heat input.

#### Melting Efficiency

Despite the simplifying assumptions inherent in Rosenthal's moving heat source equations (Ref. 16), they have proven extremely valuable in predicting fusion zone dimensions and thermal treatments to the base material during welding (Ref. 17). These equations show that the weld pool dimensions are a function of essentially only three variables: the input power, the travel speed, and the material thermal properties. There is no apparent connection between the type of heat source and these equations as long as the heat sources are capable of producing equivalent powers, and the resulting fusion zone shape for a specific heat source is such that the heat flow patterns are applicable to the equation considered. It is not surprising then to find little difference between the observed melting efficiencies for the PAW and GTAW processes as shown in Figs. 7 and 8 when the power, travel speed, material, and heat flow patterns are the same. This last point needs to be emphasized since many studies that have purported to show significant advantages for one welding process over another have erred by not comparing the processes at equivalent input powers and travel speeds, or without knowledge of the most critical variable — the net heat input.

The significantly lower melting efficiency seen for Ni 200 in Fig. 9 at the lower travel speeds can also be inferred from Rosenthal's equations and is even more directly observed in the approximation equations given by Wells (Ref. 18) for the line source (2-D heat flow) and by Okada (Ref. 19) for the point source (3-D heat flow):

$$M_l = 2\left(\frac{1}{5\left(\frac{Vd}{2\alpha}\right)} + 1\right) \quad \text{(Ref.18)} \qquad (5)$$

$$M_p = \frac{e}{2}\left[1 + \left(1 + \frac{2.6}{\left(\frac{Vd}{2\alpha}\right)^2}\right)^{1/2}\right] \quad \text{(Ref.19)} \qquad (6)$$

where: M = melting efficiency; V = travel speed; d = pool diameter; $\alpha$ = thermal diffusivity; and e = 2.71

These equations are approximations derived from Rosenthal's equations that are valid only for limited conditions but are nonetheless useful since they analytically predict how a change in thermal diffusivity or travel speed will affect the resulting melting efficiency.

The horizontal asymptote that is reached for melting efficiency at high travel speeds as shown in Figs. 7–9 has also been predicted with analytical solutions of Rosenthal's equations at the high speed limits. Wells reported a maximum melting efficiency of 0.48 for the line source and Swift-Hook and Gick (Ref. 20) reported a maximum value for the point source of 0.37. The maximum melting efficiency measured in this study was 0.46 as shown in Fig. 12, which is in good agreement with the predicted line source maximum. It is interesting to note that an approximate two-dimensional heat flow pattern is predetermined by the use of an arc process in an edge weld configuration when the entire top surface is melted.

Since two-dimensional heat flow is fundamentally more efficient in producing melting than three-dimensional heat flow, as is indicated by the above approximation equations, the extremely high values of melting efficiency reported here are in part due to the edge weld configuration. This is an important reason why edge welds are so prevalent in heat sensitive microwelding applications. Since these reported efficiencies are near the theoretical limiting value, it is expected that neither the EBW nor the LBW process will produce higher melting efficiencies in this configuration despite their significantly higher power densities.

The pulsed current GTAW welds shown in Figs. 10 and 11 indicate that an important advantage of current pulsation is the ability to achieve high melting efficiencies at slow travel speeds. This observation agrees with the results of Becker and Adams (Ref. 21) who found that the required output power for full penetration welding with GTAW decreased significantly at low travel speeds when low duty cycle current pulsation was used. As mentioned earlier, the maximum practical travel speeds are limited by humped weld beads and sometimes incomplete fusion or hot cracking, consequently, the ability to weld at slower travel speeds and still achieve high melting efficiency is an important benefit of pulsed current processes.

The probable reason why the pulsed current PAW welds in Fig. 12 did not reach a horizontal asymptote as did the pulsed current GTAW welds in Fig. 10 is because the input power was less for the pulsed current PAW welds as discussed earlier. What Fig. 12 indicates is that the optimum combination of power and travel speed was not selected for either continuous current case (duty cycle = 1.0), which resulted in an increase in melting efficiency for the lower duty cycles. Again, it should be mentioned that it is only reasonable to compare welding processes on the basis of melting efficiency at comparable output powers and travel speeds, otherwise, errors in interpretation of the data are likely.

It would be beneficial then to have a parameter that allows one to compare welding processes at equivalent powers and travel speeds, and also to normalize the dependence on base material. Then the functional dependence of melting efficiency on the parameter could be described by a single curve and used to predict the melting efficiency for any level of power, travel speed, or type of material.

Some researchers have applied dimensional analysis to this problem in the past (Refs. 22, 23) but a review of the literature on melting efficiency has found that very little empirical data (Refs. 9, 24–26) has been published. Some attempts have been made to correlate published data on fusion zone dimensions with the output power and travel speed, by the use of dimensionless groups that indicate the level of melting efficiency. Unfortunately, these analyses often rely on unsubstantiated assumptions about the energy transfer efficiency as well as the fusion zone volume, which can be the source of appreciable error. Indeed, the lack of widespread understanding about melting efficiency in the welding community (the AWS *Welding Handbook*, Ref. 27, states that EBW and LBW can achieve virtually 100% melting efficiency) is a direct result of the conflicting values for arc efficiency or energy transfer efficiency that have been published over the years. It is impossible to accurately know the melting efficiency when an incorrect determination of the arc efficiency has been made.

Attempts to correlate the melting efficiencies found in this study with the most commonly used dimensionless groups, in order to predict melting efficiency, have not been successful. The functional relationship between melting efficiency and travel speed predicted by Equations 5 and 6 is similar to the trend seen in Fig. 9, but otherwise, they do not correlate. In each case, the dimensionless groups failed to normalize the dependence of melting efficiency on the type of base material. A large divergence developed between the data sets for the two materials due to the factor of five difference in thermal diffusivity between them.

A dimensionless parameter has been determined, however, that eliminates this divergence and correlates extremely well with all the continuous current data as shown in Fig. 19. Compared to Fig. 9, it is obvious that the strong material dependence has been eliminated with this parameter and that one curve can be used to describe all the continuous current data. We will call this parameter P, and it is given by the following expression:

$$P = q\ V/\delta h\ \nu\ \alpha \quad (7)$$

where: q = net power (watts); V = travel speed (m/s); $\delta h$ = enthalpy change to melt ($J/m^3$); $\nu$ = kinematic viscosity at the melting point ($m^2/s$); and $\alpha$ = thermal diffusivity at 300 K ($m^2/s$).

It is unfortunate that some of the required material thermal property data used in this equation are difficult to obtain for even common engineering alloys such as 304 stainless steel, and sometimes must be estimated. The value of kinematic viscosity for pure nickel at the melting point was $0.62 \cdot 10^{-6}\ m^2/s$, and the estimated value used for 304 stainless steel was $0.80 \cdot 10^{-6}\ m^2/s$ (Ref. 28). The enthalpies of melting and the thermal diffusivities were given earlier. It is interesting to note that the P parameter takes into account the influence of convection in the weld pool and will increase for metals with lower liquid metal viscosity.

A linear correlation between melting efficiency and the P parameter was obtained by plotting the natural log of melting efficiency vs. the inverse of P as shown in Fig. 20. It was also found that the pre-

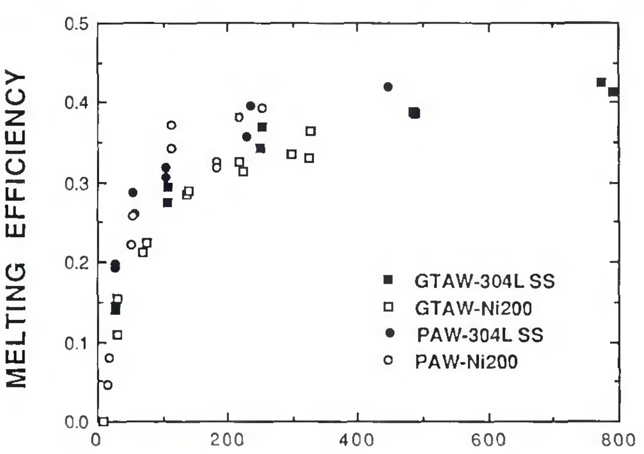


*Fig. 19 — Dependence of melting efficiency on the dimensionless parameter P for all continuous current edge welds.*

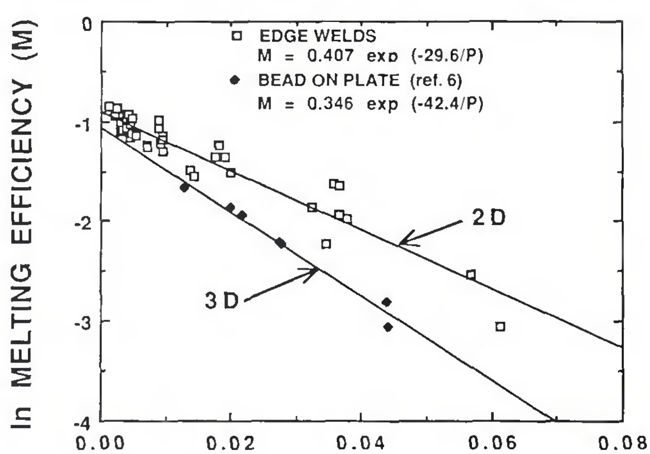


*Fig. 20 — Linear dependence of ln melting efficiency with inverse P for 2D and 3D heat flow conditions.*

viously published results (Ref. 6) for bead-on-plate welds also fit a linear correlation but had a different slope and intercept. We interpret this as an indication of the different heat flow conditions present in these two weld geometries, which is evident since bead-on-plate welds usually produce three-dimensional heat flow and edge welds usually produce two-dimensional heat flow. When the linear regression equations shown in Fig. 20 are used to compute the melting efficiency at the limit as P goes to infinity, the maximum for the edge weld configuration is 0.41 and 0.35 for the bead on plate welds. These values are in good agreement with the maximum values for the line source and point source approximations noted earlier which correspond, respectively, to two-dimensional and three-dimensional heat flow conditions as would be expected.

Based on the earlier discussion of arc efficiency and heat input, one can readily estimate what the expected net input power for a particular GTA or PA weld schedule will be. With proper selection of the applicable thermal property data, the parameter P can be determined and used with one of the equations in Fig. 20 to make a reasonable prediction of the melting efficiency. For welds that result in predominantly two-dimensional heat flow such as edge welds or full penetration welds, the edge weld equation should be used. For welds where three-dimensional heat flow occurs (such as square-groove welds), the bead-on-plate equation applies. Further work needs to be done in order to apply this technique to the pulsed current processes, since a technique for the proper selection of input power level has not been determined. It is clear though that the beneficial effect of current pulsation at low travel speeds is consistent with Fig. 19, when one realizes that the peak power always increases with decreasing duty cycle.

#### Penetration

The superior use of net heat input in achieving penetration that is exhibited in Figs. 13 to 16 by the PAW process demonstrates the increased penetrating power of the PAW torch that has helped make it so widely used in cutting applications. It was observed that a radial displacement of the weld pool by the high velocity plasma occurred, resulting in the arc impinging directly at the weld root. In contrast for the GTA welds, there was little pool displacement and the arc energy was deposited at the pool surface leading to kidney-shaped weld pools for this edge weld configuration. The radial pool displacement is characteristic of the keyhole mode PAW process and is probably required for the process to achieve its superior performance.

Comparison of Figs. 13 and 14 indicates that for the low-speed PA welds, more normalized penetration was achieved in 304 stainless steel than in Ni 200 at a given travel speed, but at the fastest travel speeds both materials reached equivalent values (about 25 mm/kJ/mm). Similar asymptotic behavior occurred for melting efficiency at the high-speed limit (Fig. 9), which is not surprising since for this edge weld geometry the volume melted is proportional to penetration. Unlike the PAW process, the normalized penetration did not increase for the GTAW process when current pulsation was used at either of the travel speeds shown in Figs. 15 and 16. This behavior is somewhat odd, since an increase in melting efficiency did occur for the slower travel speed as was shown in Fig. 10. Apparently, any beneficial effect of current pulsation appears to have been concealed both by the earlier mentioned change in heat input seen for GTAW, and by the kidney-shaped weld pools that have kept penetration from increasing. These results indicate that the increased melting efficiency that has long been known to occur with pulsed current welding is not used as effectively with the GTAW process as it is with the PAW process in the edge weld configuration examined here.

As one would expect, the normalized penetration values are low when compared to some of the best values seen for the EBW process, where exceptionally deep penetration is possible. Calculations using data in Ref. 20 indicate this parameter can be as high as 100 mm/kJ/mm, if one assumes an energy transfer efficiency of 0.85. There is a considerable manufacturing trade-off, however, when exceedingly deep and narrow welds are chosen over more symmetrically shaped ones. Standard machined part tolerances are typically so generous that it is necessary to melt wider fusion zones in order to compensate for the increased gaps and mismatch. Large depth-to-width ratios can then be impractical and fusion zone shapes similar to Fig. 18 are often preferred. Since the melting efficiency for the PAW edge weld can readily be maximized, there is little incentive then to select the higher cost process that cannot be any more efficient.

## Conclusions

1) The melting efficiencies for the GTAW and PAW processes were equivalent and increased rapidly with travel speed until reaching an asymptotic level (~41%).

2) The PAW process produced greater weld penetration at equivalent net heat inputs than the GTAW process, for the edge weld geometry examined here.

3) A dimensionless parameter, $P = q V/\delta h \nu \alpha$ has been determined that correlates well with the measured melting efficiencies for both of the weld processes and materials studied.

4) Simple monomial equations based on the experimental data have been developed, $M = 0.407\ e^{-29.6/P}$ for welds with two-dimensional heat flow, and $M = 0.346\ e^{-0.90/P}$ for welds with three-dimensional heat flow, which can predict the PAW and GTAW melting efficiency based on knowledge of the weld schedule and the material thermal properties.

5) The empirically derived equations indicate that the maximum melting efficiency is higher for edge welds than for square-groove welds, and therefore, edge welds are preferred for heat sensitive microwelding applications.

6) Melting efficiency is significantly lower for Ni 200, a relatively high thermal diffusivity material, than for 304 stainless steel, a relatively low thermal diffusivity material, except at the high-speed limit where a similar asymptotic level was reached for both materials.

7) Pulsed current can greatly improve the melting efficiency at slow travel speeds where melting efficiency is low but has no effect at fast travel speeds where it is already maximized.

8) The arc efficiency for the PAW process was found to be lower and somewhat more variable (from ~0.50 to 0.75) than the GTAW process, which tended to be constant at a value of ~0.8 for both pulsed and continuous current conditions.

9) It is postulated that the lower and more variable arc efficiencies measured for the PAW process are due to heat transfer at the torch nozzle.

10) No difference was observed between the measured arc efficiencies on 304 stainless steel and Ni 200 for a given process.

*Acknowledgments*

We would like to acknowledge Mark McAllaster and Anthony Romero for their high-quality metallographic work, which is so important in a study of this kind. We thank Warren Giedt for encouraging this work, Charles Robino for his insightful discussions, and express our appreciation to Michael Cieslak and Anthony Russo for a critical review of the manuscript. This work was performed at Sandia National Laboratories for the United States Department of Energy under contract number DE-AC04-76DP00789.

*References*

1. Omar, A. A., Lundin, C. D. 1976. Pulsed plasma-pulsed GTA arc: a study of the process variables. *Welding Journal* 58 (4):408-s to 420-s.

2. ASM International. 1983. *Metals Handbook,* Volume 6, 214-224. Materials Park, Ohio.

3. Born, K. 1981. Plasma welding. *WT-Zeitschrift fur industrielle Fertigung* (71):3-7.
4. Knorovsky, G. A., Fuerschbach, P. W. 1986. Calorimetry of pulsed vs. continuous gas tungsten arc welds. *Proc. International Conference on Trends in Welding Research*. Ed. S. A. David: 393-399. ASM International.
5. Benzinger, T. H., Kitzinger, C. 1949. Direct calorimetry by means of the gradient principle. *Rev. of Scientific Instruments* 20 (12).
6. Giedt, W. H., Tallerico, L. N., Fuerschbach, P. W. 1989. GTA welding efficiency: calorimetric and temperature field measurements. *Welding Journal* 68(1):28-s to 32-s.
7. Kelley, K. K. 1960. Contributions to the data on theoretical metallurgy: 128. Bulletin 584, U.S. Bureau of Mines.
8. Feith, A. D., Hein, C. P., Johnstone, C. P., Flagella, P. N. 1968. Thermophysical properties of low carbon 304 stainless steel to 1350°C. GEMP 643.
9. Jackson, C. E., Goodwin, W. J. 1948. Effect of variations in welding technique on the transition behavior of welded specimens. *Welding Journal* 27(5):253-s to 266-s.
10. Savage, W. F., Nippes, E. F., Agusa, K. 1979. Effect of arc force on defect formation in GTA welding. *Welding Journal* 58(7):212-s to 224-s.
11. Liebisch, H. 1978. Microplasma: precision and low energy requirements. *Welding and Metal Fabrication* 46(9):445-450.
12. Quigley, M. B. C., Richards, P. H., Swift-Hook, D. T., Gick, A. E. F. 1973. Heat flow to the workpiece from a TIG welding arc, *J. Phys. D: Appl. Phys.* 6:2250-2258.
13. Smartt, H. B., Stewart, J. A., Einerson, C. J. 1985. Heat transfer in gas tungsten arc welding. *Proc. ASM Intl. Welding Congress*, ASM 8511-011.
14. Metcalfe, J. C., Quigley, M. B. C. 1975. Heat transfer in plasma-arc welding. *Welding Journal* 54(3):99-s to 103-s.
15. Huntington, C. A., Eagar, T. W. *Laser Welding of Aluminum and Aluminum Alloys*. Cambridge, Mass., Massachusetts Institute of Technology.
16. Rosenthal, D. 1946. The theory of moving sources of heat and its application to metal treatments. *Trans. of the ASME*, 68:849-866.
17. Lancaster, J. F. 1965. *The Metallurgy of Welding, Brazing, and Soldering*. 51 Great Britain, George Allen and Unwin.
18. Wells, A. A. 1952. Heat flow in welding. *Welding Journal* 31(5):263-s to 267-s.
19. Okada, A. 1977. Application of melting efficiency and Its problems. *Journal of the Japan Welding Society* 46(2):53-61.
20. Swift-Hook, D. T., Gick, A. E. F. 1973. Penetration welding with lasers. *Welding Journal* 52(11):492-s to 499-s.
21. Becker, D. W., Adams, C. M., Jr. 1978. Investigation of pulsed GTA welding parameters, *Welding Journal* 57(5):134-s to 138-s.
22. Hablanian, M. H., 1963. A correlation of welding variables. *Proc. of the Fifth Mtg. of the Electron Beam Symposium*. ed. J. R. Morley, 262-268.
23. Berezovskii, B. M. 1979. The thermal efficiency of the process of penetrating metals with a welding arc at the surface. *Automatic Welding* 10:18-21.
24. Niles, R. W., Jackson, C. E. 1975. Weld thermal efficiency of the GTAW process. *Welding Journal* 54(1):25-s to 32-s.
25. Locke, E. V., Hoag, E. D., Hella, R. A. 1972. Deep penetration welding with high power lasers. *IEEE Journal of Quantum Electronics* QE-8(2):132-135.
26. Collings, N., Wong, K. Y., Guile, A. E. 1979. Efficiency of tungsten-inert gas arcs in very high-speed welding. *Proc. Inst. Electr. Eng.* 126,(3):276-280.
27. American Welding Society. *Welding Handbook*, Vol. 1:34. AWS, Miami, Fla.
28. Brandes, E. A., (ed.). 1983. *Smithells Metals Reference Book*, Sixth Edition:14-7, Butterworths, London, England.

# WRC Bulletin 343
# May 1989

## Destructive Examination of PVRC Weld Specimens 202, 203 and 251J

This Bulletin contains three reports:

**(1) Destructive Examination of PVRC Specimen 202 Weld Flaws by JPVRC**
**By Y. Saiga**

**(2) Destructive Examination of PVRC Nozzle Weld Specimen 203 Weld Flaws by JPVRC**
**By Y. Saiga**

**(3) Destructive Examination of PVRC Specimen 251J Weld Flaws**
**By S. Yukawa**

The sectioning and examination of Specimens 202 and 203 were sponsored by the Nondestructive Examination Committee of the Japan Pressure Vessel Research Council. The destructive examination of Specimen 251J was performed at the General Electric Company in Schenectady, N.Y., under the sponsorship of the Subcommittee on Nondestructive Examination of Pressure Components of the Pressure Vessel Research Committee of the Welding Research Council. The price of WRC Bulletin 343 is $24.00 per copy, plus $5.00 for U.S., or $8.00 for overseas, postage and handling. Orders should be sent with payment to the Welding Research Council, Room 1301, 345 E. 47th St., New York, NY 10017.

---

# WRC Bulletin 354
# June 1990

The two papers contained in this bulletin provide definitive information concerning the elevated temperature rupture behavior of 2¼Cr-1Mo weld metals.

**(1) Failure Analysis of a Service-Exposed Hot Reheat Steam Line in a Utility Steam Plant**
**By C. D. Lundin, K. K. Khan, D. Yang, S. Hilton and W. Zielke**

**(2) The Influence of Flux Composition of the Elevated Temperature Properties of Cr-Mo Submerged Arc Weldments**
**By J. F. Henry, F. V. Ellis and C. D. Lundin**

The first paper gives a detailed metallurgical failure analysis of cracking in a longitudinally welded hot reheat pipe with 184,000 hours of operation at 1050°F. The second paper defines the role of the welding flux in submerged arc welding of 2¼Cr-1Mo steel.

Publication of this report was sponsored by the Steering and Technical Committees on Piping Systems of the Pressure Vessel Research Council of the Welding Research Council. The price of WRC Bulletin 354 is $50.00 per copy, plus $5.00 for U.S. and $10.00 for overseas postage and handling. Orders should be sent with payment to the Welding Research Council. 345 E. 47th St., Room 1301, New York, NY 10017.